This is a preprint, the final version is subject to change, of the American Mineralogist (MSA)
Cite as Authors (Year) Title. American Mineralogist, in press.
DOI: https://doi.org/10.2138/am-2019-6719

Revision1

Zinc transport in hydrothermal fluids: on the roles of pressure and sulfur versus chlorine complexing

Barbara Etschmann[1], Weihua Liu[2], Robert Mayanovic[3], Yuan Mei[2], Steven Heald[4], Robert Gordon[5] and Joël Brugger[1]

1. School of Earth, Atmosphere and Environment, Monash University, Clayton, VIC, 3800, Australia
2. CSIRO Mineral Resources Flagship, Clayton, VIC 3168, Australia
3. Department of Physics Astronomy and Materials Science, Missouri State University, Springfield, MO 65897, USA
4. Advanced Photon Source, Argonne National Laboratory, Lemont, IL 60439, USA
5. Moyie Institute & Dept. of Physics, Simon Fraser University, Burnaby, BC, Canada

Abstract

We provide an experimental confirmation of the suggestion, based on thermodynamic simulations and extrapolations (Zhong et al. 2015), that Zn is transported in the form of chloride complexes in most acidic, shallow hydrothermal systems; while bisulfide complexes become increasingly important in deep, pH neutral to basic hydrothermal systems. We used *in situ* X-ray absorption spectroscopy (XAS) diamond anvil cell experiments to determine Zn(II) speciation in a 1 m NaHS + 0.2 m HCl solution in contact with sphalerite. XANES data indicate that Zn coordinates to oxy/hydroxyl/chloride ligands from room temperature up to and including 200 °C, and then at higher temperatures (≥ 300 °C) and pressures (> 2 kbar) changes to complexing with sulfur. Our data confirm that bisulfide complexes become increasingly important in neutral-alkaline solutions at high pressure and temperature, due to an increase in sulfur solubility and to favorable entropy contributions for bisulfide versus chloride complexes.

Keywords: Zinc, Sulfur, Chloride, Hydrothermal, High temperature and pressure.

This is a preprint, the final version is subject to change, of the American Mineralogist (MSA)
Cite as Authors (Year) Title. American Mineralogist, in press.
DOI: https://doi.org/10.2138/am-2019-6719

Introduction

Knowledge of metal complexation is important for predicting the solubility, transport and deposition of metals leading to the formation of hydrothermal ore deposits. Most zinc (Zn) deposits share a hydrothermal origin. As chloride is the most abundant anion in hydrothermal fluids (Yardley, 2005) and the sulfide mineral sphalerite (ZnS) is by far the most important Zn ore mineral, the complexation of Zn(II) with chloride and sulfur ligands has been studied extensively (Ruaya and Seward, 1986; Bourcier and Barnes, 1987; Plyasunov and Ivanov, 1991; Anderson et al., 1998; Tagirov et al., 2007; Tagirov and Seward, 2010).

Advances in *in situ* synchrotron-based X-ray absorption spectroscopy (XAS) and *ab initio* molecular dynamics simulations (AIMD) provide us with increasingly reliable views of the speciation and thermodynamics of metal complexes at the molecular level (Brugger et al., 2016). For example, Mei et al. (2015) combined AIMD simulations with *in situ* XAS data to demonstrate that Zn(II) is bonded to Cl predominantly in a tetrahedral geometry up to 400 ^{o}C and 1 kbar, with a trigonal planar geometry appearing above 500 ^{o}C (35% trigonal planar at 600 ^{o}C), and were able to use this new speciation model to reinterpret available solubility data (e.g., Ruaya and Seward, 1986; Bourcier and Barnes, 1987), demonstrating that discrepancies among the different interpretations of the experimental data arose from erroneous assumptions about Zn(II) complexing rather than experimental errors. A subsequent study (Mei et al., 2016) demonstrated that Zn is coordinated with S in tetrahedral $[Zn(HS)_n(H_2O)_{4-n}]^{2-n}$ complexes up to 300 ^{o}C and 1 kbar, with trigonal planar species predicted to become predominant at lower temperatures than in chloride solutions (i.e., at 400-500 ^{o}C for Zn in a 2 m NaHS solution).

The thermodynamic properties proposed by Mei et al. (2015, 2016) suggest that Zn(II) bisulfide complexes grow in importance with increasing temperature in neutral-alkaline solutions, while chloride species are dominant at lower temperatures. This is consistent with the geochemical modeling of Zhong et al. (2015a) that predicted that chloride complexes will predominate in most shallow(< ~4 km) rock-buffered hydrothermal systems, while bisulfide

This is a preprint, the final version is subject to change, of the American Mineralogist (MSA)
Cite as Authors (Year) Title. American Mineralogist, in press.
DOI: https://doi.org/10.2138/am-2019-6719

55 complexes become increasingly important at high PT (> 10 km), due to an increase in sulfur
56 solubility (>3 molal at T ≥ 500 ˚C) and favorable entropy contributions for bisulfide versus
57 chloride complexes in aqueous fluids (Mei et al., 2013). These predictions are based on data
58 collected in fluids containing either chloride or hydrosulfide. The aim of this study is to test the
59 above predictions and determine the predominant Zn species in a mixed Cl + S fluid.

60 **Experimental Methods**

61 X-ray Absorption Near Edge Structure (XANES) data were collected using a
62 Hydrothermal Diamond Anvil Cell (HDAC) at beamline 20-ID at the Advanced Photon Source
63 (APS) at Argonne National Lab, Illinois. The APS is a 7 GeV ring with a maximum current of
64 102 mA. Beamline 20-ID is an undulator beamline with a Si(111) monochromator with an
65 energy resolution ($\Delta E/E$) of 1.4 x 10^{-4} (at 10 keV). A focused beam size of 5 μm^2 was used. The
66 incident and transmitted beam intensities I_0 and I_1 were measured using ion chambers. A 4-
67 element Si-drift detector, used for detecting fluorescence data, was positioned at 90° to the
68 incident X-ray beam.
69 Solutions were prepared using: NaHS(s) (Alfa Aesar), $ZnBr_2$ (GFS, reagent grade), S (Alfa
70 Aesar, 99.5 %), $ZnCl_2$ (Sigma, reagent grade), HBr (48%, Sigma) and HCl (37% Sigma). The
71 requisite amounts were diluted/dissolved in water to prepare the solutions listed in Table 1. A
72 stopped PTFE solution cell was used to measure XAS data for the standard solution (Sol2,
73 Table 1) under ambient conditions, to aid comparison with data collected previously at 1 kbar at
74 the European Synchrotron Research Facility (ESRF; Grenoble, France) (Mei et al. 2016).
75 Solutions were loaded with a small piece of sphalerite (Picos del Europa mine, Spain; sample
76 M4983, Museum Victoria) into the modified Bassett-style HDAC (Bassett et al., 2000, Yan et
77 al., 2011). XANES data were collected *in situ* up to 500 ^{o}C and ~4.5 kbar upon heating. The
78 solution, loaded using a micro syringe, was contained in a cylindrical hole (500 µm in diameter)
79 drilled in a Rhenium gasket of 125 µm thickness (Figure 1). Similar to previous studies (e.g.,
80 Mayanovic et al., 2002), the HDAC was mounted on a rotating stage on the XAS experimental

This is a preprint, the final version is subject to change, of the American Mineralogist (MSA)
Cite as Authors (Year) Title. American Mineralogist, in press.
DOI: https://doi.org/10.2138/am-2019-6719

table with a vertical optical window, allowing simultaneous optical observation of the sample from the top using a microscope and video camera, and XAS measurement with the X-ray beam entering horizontally from the side via a laser-drilled recess (150 µm diameter, 100 µm deep) through one of the anvils (Figure 1a,b). A temperature controller (PES Enterprises Inc.) was used to control the temperature to within ±1 ˚C, based on two thermocouples positioned next to the bottom and top diamonds and sealed with zirconia cement. The pressure at elevated temperature was approximated using the equation of state (EOS) of sodium chloride solutions (Driesner and Heinrich, 2007) with similar stoichiometric ionic strength as the experimental solutions, based on the observed homogenization temperatures (Table 1).

As noted in previous HDAC studies (e.g., Mayanovic et al., 1999; Bassett et al., 2000; Hong et al., 2009), diffraction from the diamond interferes with the XAS signal. To overcome this, the HDAC was rotated and spectra were collected at a number of angles with differences of 1-3˚. Changing the angle changes the location of the diffraction peaks, allowing the data to be deglitched following the procedures described by Mayanovic et al. (1999) and Hong et al. (2009).

Ab initio Molecular Dynamics Simulations

To extend the pressure range beyond those in the experiments to conditions typical of lower crust/upper mantle and shallow subduction zones, AIMD simulations of Zn(II)-Cl-HS complexes were run at 100 ºC, 1.5 kbar and 500 ºC, 1.5-20 kbar. AIMD simulations were performed using the Car-Parrinello MD code "CPMD" version 3.17.1 (Car and Parrinello, 1985). A box containing 1 Zn^{2+}, 5 HS^{-}, 1 Cl^{-}, 4 Na^{+}, 111 H_2O was used for each simulation. Details of the calculation procedures are given in Mei et al. (2015, 2016).

XANES Results

XANES spectra reflect (i) the oxidation state of the target atom, (ii) the geometry and (iii) composition (nature of ligands) of the surrounding coordination sphere. The positions of the absorption edge and of the white line (historically defined as the most intense peak just above

This is a preprint, the final version is subject to change, of the American Mineralogist (MSA)
Cite as Authors (Year) Title. American Mineralogist, in press.
DOI: https://doi.org/10.2138/am-2019-6719

the edge in the spectrum) tend to shift as a function of these parameters (Bunker, 2010; Penner-Hahn, 2005). These shifts can be accounted for electrostatically: (i) the higher the oxidation state, the higher the charge on the target atom, and the higher the X-ray energy required to eject a core electron. (ii) Six ligands will induce a higher charge in the vicinity of the central atom compared to four ligands; thus, octahedral complexes tend to have a white line at a higher energy than tetrahedral complexes. (iii) Metal-bisulfide complexes tend to have a white line at a lower energy than metal-oxide/halide complexes. S has a lower electronegativity than O/Cl, so it induces a lower formal charge on the metal atom.

Figure 1c,d shows the stacked normalized XANES spectra, and Figure 1e,f shows the stacked first derivative of the XANES of Zn in $H_2O/OH^-/Cl^-/HS^-$ solutions (Table 1). Data shown in Figures 1c,e were collected previously using a large volume autoclave (Mei et al., 2015, 2016) and clearly demonstrate the shift to lower energy in both the white line and the position of the peak of the first derivative of the XANES due to a change in the geometry of the complexes, from octahedral to tetrahedral to trigonal planar (SolsB, C, D; see Table 1), followed by a further shift to lower energies when the complexing ligand is changed to HS^- (SolE) from $Cl^-/H_2O/OH^-$, with increasing temperature. Sphalerite solubility in SolE was estimated to be 13(3) mmolal at 500˚C, 1 kbar, which compares well with the predictions using Zn bisulfide complexes properties from Mei et al. (2016) (70 mmolal; details in Table 1).

Reassuringly, the data collected with the HDAC show the same trend as those collected with the large volume autoclave (Figure 1c-f). The results for the Cl-free Sol10 (sphalerite + 2 m NaHS + S) are identical to those collected previously (SolE), and indicate the presence of Zn(II) bisulfide complexes at high temperature as a result of prograde solubility. It should be noted that it was necessary to add extra S into the system for Sol10 (HDAC) compared to SolE (autoclave). Attempts using just the NaHS solution + sphalerite resulted in the dissolution of the Re gasket; geochemical modeling demonstrated that the S-free solution (e.g., $pH_{400^\circ C}$=7.5) is much more basic than the S-bearing solution ($pH_{400^\circ C}$=4.4). Excess sulfur both ensures buffering

This is a preprint, the final version is subject to change, of the American Mineralogist (MSA)
Cite as Authors (Year) Title. American Mineralogist, in press.
DOI: https://doi.org/10.2138/am-2019-6719

of the S content of the fluid despite reaction with the gasket, and a pH closer to neutral (4.8 @ 400 ˚C, 2.95 kbar).

The only source of sulfur in Sol6 (sphalerite in 0.2 m HCl) was due to the dissolution of sphalerite. Under these conditions the concentration of available chlorine was so much higher than that of sulfur that it dominated complexation to Zn; acidic pH also decreases the stability of bisulfide complexes, since H_2S(aq) predominates over HS^- (reaction $HS^- + H^+ = H_2S$(aq)).

The most exciting result from the HDAC experiments is that Sol5 (sphalerite in 1 m NaHS + 0.2 m HCl) clearly demonstrates a change in ligand type from ambient up to and including 200 °C to HS^- (from 300 °C and above). Note that according to available thermodynamic properties (review in Zhong et al. 2015, supplemented by Mei et al. 2015, 2016), Zn bisulfide complexes should dominate Zn speciation even at room T in Sol5; given the basic pH of the solution (Table 1), and given the small amount of experimental data available under these conditions (Tagirov and Seward 2010), this could indicate the importance of hydroxide complexes yet to be fully characterized.

AIMD Results

The results of simulations of Zn(II) speciation in solutions containing 2.5 m HS^- and 0.5 m Cl^- at experimental pressures and at 20 kbar are listed in Table 2. The simulations show that (i) at 100 °C, 1.5 kbar, four-fold tetrahedral complexes are stable; (ii) at 500 °C, 1.5 and 4.5 kbar three-fold complexes predominate with four-fold complexes being present for a small percentage of the time; and (iii) at 500 °C, 20 kbar four-fold species once again predominate. It was not possible to observe ligand exchange between $Cl^-/HS^-/H_2O$ as the exchange kinetics are too slow to be observed by AIMD on the scale of picoseconds, even at elevated temperatures (Mei et al., 2015, 2016).

At low pressures (≤ 4.5 kbar), the AIMD results are consistent with experimental measurements. The increase in coordination from three ($Zn(HS)_3^-$) to four ($Zn(HS)_4^{2-}$) ligands of the Zn bisulfide complexes with increasing pressure is similar to that observed previously with

This is a preprint, the final version is subject to change, of the American Mineralogist (MSA)
Cite as Authors (Year) Title. American Mineralogist, in press.
DOI: https://doi.org/10.2138/am-2019-6719

159 increasing HS^- concentration (Mei et al., 2016). Much like higher HS^- concentrations, higher
160 pressures enhance the stability of the $Zn(HS)_4^{2-}$ complex, which in turn enhances Zn solubility
161 in sulfur-rich fluids at high pressures.

162 **Discussion**

163 The hypothesis offered by Zhong et al. (2015a), stating that chloride is the dominant
164 ligand controlling Zn mass transfer at low PT conditions whereas sulfur becomes increasingly
165 important at higher PT conditions, has been verified experimentally. Our XANES results show
166 that when sufficient sulfur and chlorine are available, in neutral-alkaline solutions, Zn bonds
167 preferentially to OH^-/H2O/Cl^- at lower PT conditions and then with HS^- with increasing PT
168 conditions, (e.g., Sol5, calculated pH_25˚C = 7.4).

169 This can be accounted for on a macroscopic scale by noting that the reduction of the
170 dielectric constant of water with increasing temperature (from 78 at 25 ^oC to 18.3 at 500 ^oC and
171 4.5 kbar, Fernandez et al, 1995) drives complexing of metal species towards having lower
172 overall charge (eventually neutral charge) with increasing temperature. This can be achieved in
173 two ways: (i) the geometry changes from octahedral to tetrahedral to trigonal, thereby
174 decreasing the overall charge of the complex, and, (ii) the bond polarity decreases, i.e. Zn will
175 preferentially bond with ligands with decreasing electronegativity with increasing temperature
176 (Pauling electronegativity: Zn=1.65, O = 3.44, Cl = 3.16, S = 2.58).

177 On a microscopic level, the increase in entropy associated with (i) reduction in
178 coordination number (Crerar et al., 1985; Susak and Crerar, 1985) and/or (ii) reduction of the
179 number of hydration waters (i.e., less solvation) of Cl^- and HS^- is the impetus for forming these
180 metal-Cl^-/HS^- complexes (Sherman, 2010). The reduction of hydration waters of HS^- is larger
181 than that of Cl^- (Sherman, 2010; Mei et al., 2013) resulting in a preference for complexing to
182 HS^- compared to Cl^-. In these and previous experiments (Mei et al., 2015, 2016), it was found
183 that Zn speciation transitions to a lower coordination with S (trigonal complex at 300 ^oC to
184 400 ^oC) at a lower temperature than with Cl (evidence for trigonal complex around 500 ^oC).

This is a preprint, the final version is subject to change, of the American Mineralogist (MSA)
Cite as Authors (Year) Title. American Mineralogist, in press.
DOI: https://doi.org/10.2138/am-2019-6719

185 However, this is the first direct experimental demonstration that given sufficient amounts of Cl
186 and S in the aqueous system, Zn undergoes a transformation from predominant chloro/aqua ion
187 to bisulfide complexing with increasing P and T conditions.

188 AIMD calculations show that at 20 kbar the coordination of Zn(II) reverts towards
189 tetrahedral, which is associated with an increase in the number of bisulfide ligands coordinated
190 to Zn. The effect of pressure on mineral solubility is complex (e.g. Crerar et al. 1985; Brugger et
191 al., 2016). The type of coordination change affecting Zn complexing as a function of pressure is
192 not taken into account by popular extrapolation algorithms (e.g., Sverjensky et al. 2014). In this
193 case, the change in coordination will tend to increase Zn solubility in S-rich fluids with
194 increasing pressure: MD simulations suggest that this effect counterbalances a general trend
195 towards stronger dissociation at high pressures (Seward and Barnes, 1997) driven by pressure-
196 dependent changes (i.e. solution density) in the hydration of the free ions (Cl^- and HS^-).

197 **Implications**

198 The new experiments provide the first experimental confirmation that Zn(II) bisulfide
199 complexes may dominate Zn transport in high temperature neutral-alkaline fluids, including
200 metamorphic fluids (e.g., Zhong et al., 2015b, Mei et al., 2016). MD simulations suggest that
201 pressure-driven coordination changes may be important in controlling Zn speciation (and hence
202 solubility) in deep geological fluids, e.g. subduction zones. Sulfate/polysulfide/bisulfide
203 equilibria in subduction zone is a subject of intense scrutiny and debate (e.g., Debret and
204 Sverjensky; 2017; Rielli et al. 2017). Pons et al. (2016) used the fact that the fractionation of
205 stable Zn isotope between mineral and fluid is sensitive to the predominant Zn(II) complexes
206 (Fuji et al., 2011) to infer that Zn(II) sulfate complexes may be important for Zn transfer from
207 slab to mantle as a result of slab dehydration and deuteric mantle metasomatism. Debret and
208 Sverjensky (2017) used thermodynamic modeling to show that the predominance of sulfate
209 versus bisulfide ligand in fluids resulting from serpentinite dehydration depends upon the
210 amount of dissolved sulfide (pyrrhotite) at 20 kbar and 630-660˚C. Our study confirms that

under conditions where reduced sulfur predominates in solution, $Zn(HS)_4^{2-}$ (Fuji et al., 2011) and/or $Zn(HS)_3^{2-}$ (Mei et al., 2016) are the most likely Zn complexes accounting for Zn mobility.

Acknowledgements

We thank the APS (Sector 20) for beam time and Museum Victoria for supplying the sphalerite. We acknowledge travel funding provided by the ISAP, Australian Synchrotron, funded by the Australian Government. The AIMD calculations were supported by the Pawsey Supercomputing Centre, with funding from the Australian and Western Australian Governments. W.L. is a recipient of ARC Future Fellowship (FT130100510). We are grateful to Marion Louvel and two anonymous reviewers for helping us to improve this manuscript.

References

Anderson, A.J., Mayanovic, R.A. and Bajt, S. (1998) A microbeam XAFS study of aqueous chlorozinc complexing to 430 ˚C in fluid inclusions from the Knaumühle granitic pegmatite, Saxonian granulite facies, Germany. Canadian Mineralogist 36, 511-524.

Bassett, W.A., Anderson, A.J., Mayanovic, R.A. and Chou, I.M. (2000) Hydrothermal diamond anvil cell for XAFS studies of first-row transition elements in aqueous solution up to supercritical conditions. Chemical Geology 167, 3-10.

Bourcier, W.L. and Barnes, H.L. (1987) Ore Solution Chemistry - VII. Stabilities of chloride and bisulfide complexes of zinc to 350˚C. Economic Geology 82, 1839-1863.

Brugger, J., Liu, W.H., Etschmann, B., Mei, Y., Sherman, D.M. and Testemale, D. (2016) A review of the coordination chemistry of hydrothermal systems, or do coordination changes make ore deposits? Chemical Geology 447, 219-253.

Bunker, G. (2010). *Introduction to XAFS: A Practical Guide to X-ray Absorption Fine Structure Spectroscopy*. Cambridge, Cambridge University Press, 260 pp.

Car, R. and Parrinello, M. (1985) Unified Approach for Molecular Dynamics and Density-Functional Theory. Physical Review Letters 55, 2471-2474.

236 Crerar, D., Wood, S. and Brantley, S. (1985) Chemical controls on solubility of ore-forming
237 minerals in hydrothermal solutions. Canadian Mineralogist 23, 333-352.
238 Debret, B. and Sverjensky, D.A. (2017) Highly oxidising fluids generated during serpentinite
239 breakdown in subduction zones. Scientific Reports 7.
240 Driesner T., and Heinrich C.A. (2007): The System H_2O-NaCl. I. Correlation Formulae for
241 Phase Relations in Temperature-Pressure-Composition Space from 0 to 1000 °C, 0 to
242 5000 bar, and 0 to 1 X_{NaCl}. Geochimica et Cosmochimica Acta 71, 4880-4901.
243 Fernandez, D.P., Mulev, Y. Goodwin, A.R.H. and Levelt-Sengers, J.M.H. (1995) Database for
244 the static dielectric constant of water and steam. J. Phys. Chem. Ref. Data. 24., 33-69.
245 Fujii, T., Moynier, F. Pons, M.L. and Albarède, F. (2013) The origin of Zn isotope fractionation
246 in sulfides. Geochimica et Cosmochimica Acta 75, 7632-7643.
247 Hong, X.G., Newville, M., Prakapenka, V.B., Rivers, M.L. and Sutton, S.R. (2009) High quality
248 x-ray absorption spectroscopy measurements with long energy range at high pressure using
249 diamond anvil cell. Review of Scientific Instruments 80.
250 Mayanovic, R.A., Jayanetti, S., Anderson, A.J., Bassett, WA, and Chou, I.-M. (2002) The
251 structure of Yb^{3+} aquo ion and chloro complexes in aqueous solutions at up to 500 °C and
252 270 MPa. Journal of Physical Chemistry A 106, 6591-6599.
253 Mayanovic, R.A., Anderson, A.J., Bassett, W.A. and Chou, I.M. (1999) XAFS measurements on
254 zinc chloride aqueous solutions from ambient to supercritical conditions using the diamond
255 anvil cell. Journal of Synchrotron Radiation 6, 195-197.
256 Mei, Y., Etschmann, B., Liu, W., Sherman, D.M., Testemale, D. and Brugger, J. (2016)
257 Speciation and thermodynamic properties of zinc in sulfur-rich hydrothermal fluids: Insights
258 from ab initio molecular dynamics simulations and X-ray absorption spectroscopy.
259 Geochimica Et Cosmochimica Acta 179, 32-52.

Mei, Y., Sherman, D.M., Liu, W., Etschmann, B., Testemale, D. and Brugger, J. (2015) Zinc complexation in chloride-rich hydrothermal fluids (25-600 ˚C): A thermodynamic model derived from ab initio molecular dynamics. Geochimica Et Cosmochimica Acta 150, 265-284.

Mei, Y., Sherman, D.M., Liu, W.H. and Brugger, J. (2013) Ab initio molecular dynamics simulation and free energy exploration of copper(I) complexation by chloride and bisulfide in hydrothermal fluids. Geochimica Et Cosmochimica Acta 102, 45-64.

Penner-Hahn, James E. (May 2005) X-ray Absorption Spectroscopy. In: eLS. John Wiley & Sons Ltd, Chichester. http://www.els.net [doi: 10.1038/npg.els.0002984]

Plyasunov, A.V. and Ivanov, I.P. (1991) The solubility of zinc oxide in sodium chloride solutions up to 600˚C and 1000 bar. Geochemistry International 28, 77-90.

Pokrovski, G.S., Roux, J., Hazemann, J.L., and Testemale, D. (2005) An X-ray absorption spectroscopy study of argutite solubility and aqueous Ge(IV) speciation in hydrothermal fluids to 500 ˚C and 400 bar. Chemical Geology, 217(1-2), 127-145.

Pons, M.L., Debret, B., Bouilhol, P., Delacour, A. and Williams, H. (2016) Zinc isotope evidence for sulfate-rich fluid transfer across subduction zones. Nature Communications 7.

Ravel, B. and Newville, M. (2005) ATHENA, ARTEMIS, HEPHAESTUS: data analysis for X-ray absorption spectroscopy using IFEFFIT. Journal of Synchrotron Radiation 12, 537–541.

Rielli, A., Tomkins, A.G., Nebel, O., Brugger, J., Etschmann, B., Zhong, R., Yaxley, G.M. and Paterson, D. (2017) Evidence of sub-arc mantle oxidation by sulphur and carbon. Geochemical Perspectives Letters 3, 124-132.

Ruaya, J.R. and Seward, T.M. (1986) The stability of chlorozinc(II) complexes in hydrothermal solutions up to 350˚C. Geochimica et Cosmochimica Acta 50, 651-661.

Seward, T.M. and Barnes, H.L. (1997) Chapter 9: Metal Transport by Hydrothermal Ore Fluids, in: Barnes, H.L. (Ed.), Geochemistry of hydrothermal ore deposits. John Wiley & Sons, pp. 435-486.

285 Sherman, D.M. (2010) Metal complexation and ion association in hydrothermal fluids: insights
286 from quantum chemistry and molecular dynamics. Geofluids 10, 41-57.
287 Susak, N.J. and Crerar, D.A. (1985) Spectra and coordination changes of transition metals in
288 hydrothermal solutions: Implications for ore genesis. Geochimica et Cosmochimica Acta 49,
289 555-564.
290 Sverjensky, D.A., Harrison, B. and Azzolini, D. (2014) Water in the deep Earth: the dielectric
291 constant and the solubilities of quartz and corundum to 60 kb and 1200 ˚C. Geochim.
292 Cosmochim. Acta 129, 125-145.
293 Tagirov, B.R. and Seward, T.M. (2010) Hydrosulfide/sulfide complexes of zinc to 250˚C and
294 the thermodynamic properties of sphalerite. Chemical Geology 269, 301-311.
295 Tagirov, B.R., Suleimenov, O.M. and Seward, T.M. (2007) Zinc complexation in aqueous
296 sulfide solutions: determination of the stoichiometry and stability of complexes via ZnS(cr)
297 solubility measurements at 100 °C and 150 bars. Geochim Cosmochim. Acta 71, 4942-4953.
298 WaveMetrics, 2014 IGOR Pro, www.wavemetrics.com
299 Yan, H., Mayanovic, R.A., Anderson, A.J. and Meredith, P.R. (2011) An *in situ* X-ray
300 spectroscopic study of Mo^{6+} speciation in supercritical aqueous solutions. Nuclear
301 Instruments & Methods in Physics Research Section a-Accelerators Spectrometers Detectors
302 and Associated Equipment 649, 207-209.
303 Yardley, B.W.D. (2005) Metal concentrations in crustal fluids and their relationship to ore
304 formation. Econ. Geol. 100, 613-632.
305 Zhong, R., Brugger, J., Chen, Y. and Li, W. (2015a) Contrasting regimes of Cu, Zn and Pb
306 transport in ore-forming hydrothermal fluids. Chem. Geol. 395, 154-164.
307 Zhong, R., Brugger, J., Tomkins, A.G., Chen, Y. and Li, W. (2015b) Fate of gold and base
308 metals during metamorphic devolatilization of a pelite. Geochimica et Cosmochimica
309 Acta 171, 338-352.

Figure 1. (a) Experimental setup on beamline 20-ID. (b) View of sample containing solid and air bubble. The sample is located in a 500 µm Re-gasket. The diamond is fluorescent under the X-ray beam; as a result the outer edge of the diamond is "glowing", and the green line across shows X-rays travelling through the diamond above the gasket. The black circle in the center is a recess drilled into the top diamond, which allows for solution measurement by the micro-beam travelling parallel to the gasket. (c-d) Stacked the normalized XANES spectra (c) previously published data collected in large volume autoclave (Mei et al., 2015, 2016) and (d) HDAC data. **(e-f)** Stacked first derivative of the normalized XANES spectra (e) large volume and (f) HDAC data. Note the white line and the maximum of the first derivative shifts to lower energy with decreasing coordination number and ligand (S vs O/Cl).

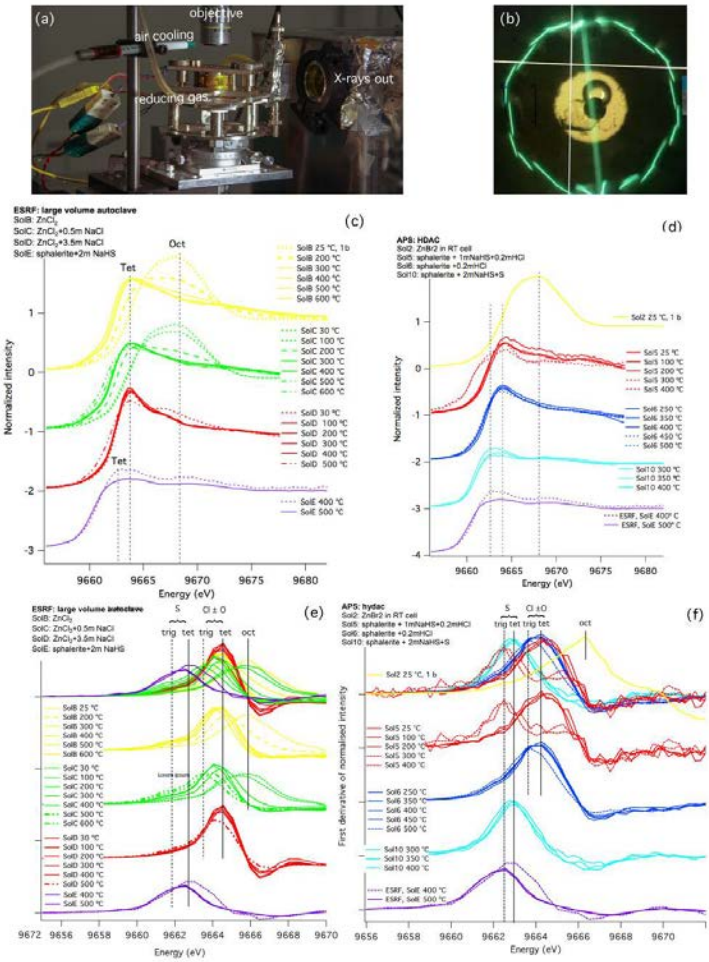

Table 1. Solution compositions for HDAC (APS) and large volume autoclave (ESRF) experiments

APS-HDAC experiments			Max T,P*	Calculated pH, Eh
Sol2 (RT cell)	0.12 g $ZnBr_2$ in 1.16 m NaBr + 0.002 m HBr		Room temperature	$pH_{25°C}$ = 2.8
Sol5	Sphalerite in 1.03 m NaHS + 0.20 m HCl	Th = 211 °C, density ~ 0.85	500 °C, P ~ 4.5 kbar	$pH_{25°C}$ = 7.4 $pH_{500°C}$ = 6.7 $Eh_{500°C}$ = -1.08
Sol6	Sphalerite in 0.20 m HCl	Th = 218 °C, density ~ 0.85	500 °C, P ~ 4.5 kbar	$pH_{25°C}$ = 0.8 $pH_{500°C}$ = 1.9 $Eh_{500°C}$ = -0.27
Sol10	Sphalerite in 1.84 m NaHS + excess S	Th = 229 °C, density ~ 0.91	400 °C, P ~ 2.95 kbar	$pH_{25°C}$ = 7.8 $pH_{400°C}$ = 4.4 $Eh_{400°C}$ = -0.50
ESRF - large volume autoclave (FAME cell) experiments. Solutions A-D were acidified to prevent hydrolyzed complexes.				
SolA	$ZnBr_2$ in 0 m NaBr + 0.01 m HBr		600 °C, 1 kbar	$pH_{25°C}$ = 2.0 pH_600°C = 2.3
SolB	$ZnCl_2$ in 0 m NaCl + 0.01 m HCl	Mei et al. 2015	500 °C, 1 kbar	$pH_{25°C}$ = 2.1 pH_500°C = 2.7
SolC	$ZnCl_2$ in 0.5 m NaCl + 0.01 m HCl	Mei et al. 2015	600 °C, 1 kbar	$pH_{25°C}$ = 2.1 $pH_{600°C}$ = 5.4
SolD	$ZnCl_2$ in 3.5 m NaCl + 0.01 m HCl	Mei et al. 2015	500 °C, 1 kbar	$pH_{25°C}$ = 2.2 $pH_{500°C}$ = 4.6
SolE*	ZnS in 2m NaHS	Mei et al. 2016	500 °C, 1 kbar	$pH_{25°C}$ = 10.3 $Eh_{25°C}$C = -0.53 $pH_{500°C}$ = 10.0 $Eh_{500°C}$ = -1.58

* Zinc solubility at 500 ˚C, 1 kbar was estimated to be 13(3) mmolal (850 ppm), based on the step height in transmission. This compares to 70 mmolal predicted using the properties from Zn-bisulfide complexes of Mei et al. (2016), and 338 mmolal using those of Tagirov 2010). For all other conditions (ESRF data), solubility was below detection limit based on transmission (≤ 3 mmolal).

Solubility was calculated following $\Delta u = \Delta\sigma.l.M.m.d$ (Pokrovski et al., 2005), where Δu is step height = 0.05(1); $\Delta\sigma$ is the difference in X-ray cross section for Zn before (9600 eV) and after (9700 eV) the edge = 215.3 cm^2/g; l is path length = 0.4 cm; M is atomic mass of Zn = 0.06538 kg/mol; m is the molal concentration of Zn in solution (mol/kg); and d is the density of fluid, estimated to be similar to that of a 2 m NaCl @ 500 °C, 1 kbar) = 0.66 g/cc (Driesner and Heinrich, 2007).

337
338
339 **Table 2**. Simulation results of Zn(II)-Cl/HS complexes at high pressure

Job ID	T (ºC)	P (kbar)	Total time (ps)	Initial configuration	Stabilization time (ps)	Stable species	Zn-S			Zn-Cl			Zn-O			CN_{tot}
							N	r	σ^2	N	r	σ^2	N	r	σ^2	
1a¶	100	1.5	14.44	$Zn(H_2O)_5Cl^+$	2.32	$Zn(H_2O)_3Cl^+$	0	-	-	1	2.23	0.0046	3	2.00	0.0067	4
1b	100	1.5	14.32	$Zn(H_2O)_5(HS)^+$	1.45	$Zn(H_2O)_3(HS)^+$	1	2.25	0.0045	0	-	-	3	2.02	0.0078	4
1c	100	1.5	14.58	$Zn(H_2O)_6^{2+}$	5.08	$Zn(H_2O)_4^{2+}$	0	-	-	0	-	-	4	1.97	0.0054	4
2	500	1.5	14.43	$Zn(HS)_3^-$	1.45	$Zn(HS)_3^-$	3	2.28	0.0160	0	-	-	0.16	2.10	-	3.16
3	500	4.5	15.01	$Zn(HS)_3^-$	1.45	$Zn(HS)_3^-$	3	2.26	0.0125	0	-	-	0.17	2.33	-	3.17
4a	500	20	15.94	$Zn(HS)_3^-$	7.62	$Zn(HS)_4^{2-}$	4	2.32	0.0195	0	-	-	0	0	-	4
4b	500	20	15.86	$Zn(H_2O)_6^{2+}$	4.35	$Zn(HS)_2O_{1-2}^*$	2	2.26	0.0126	0	-	-	1.68	1.97	-	3.68

340 * $O=H_2O/OH^-$

341 ¶Elemental solution composition: 1 Zn^{2+}, 5 HS^-, 1 Cl^-, 4 Na, 111 H_2O.
342
343

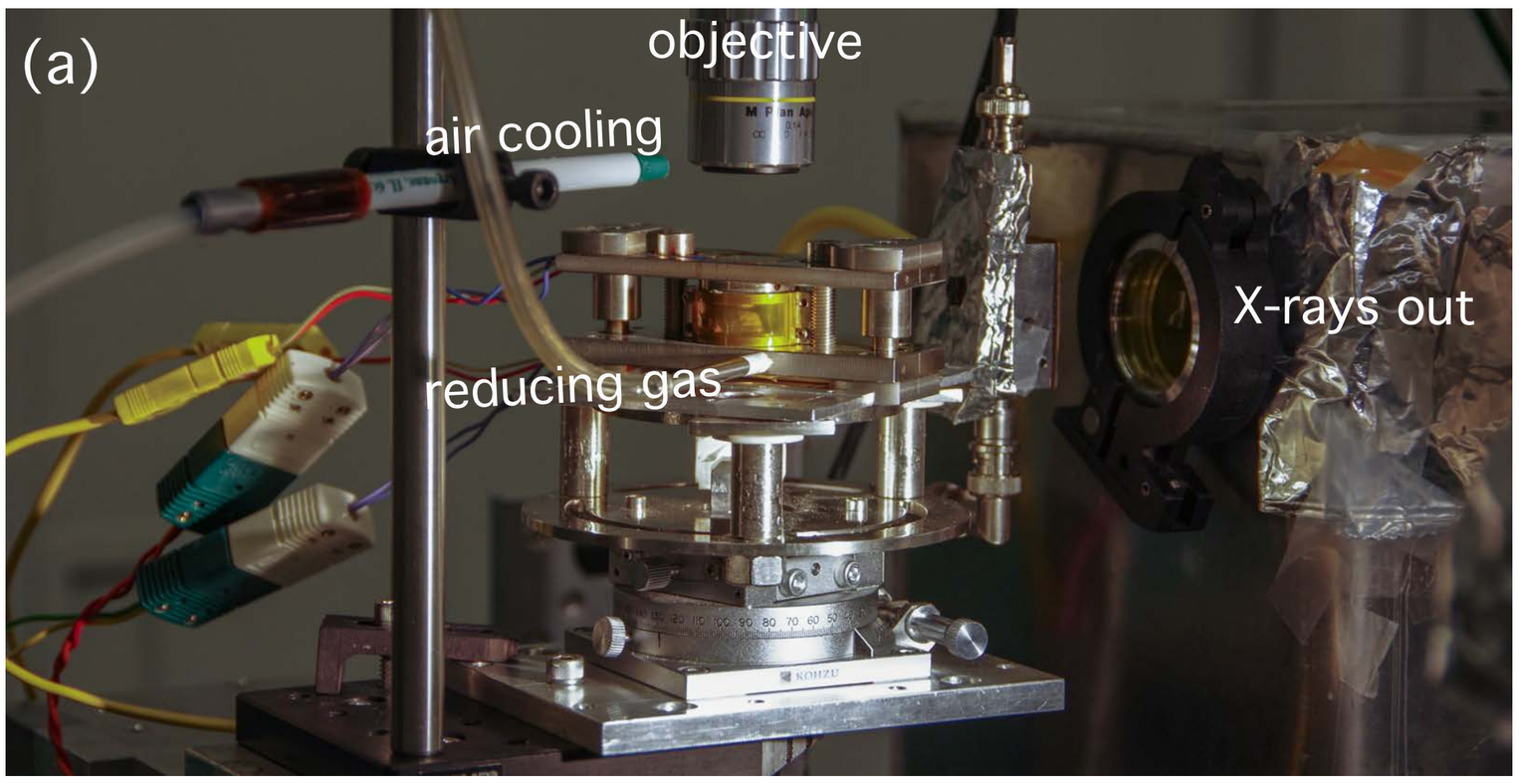
(a)
objective
air cooling
reducing gas
X-rays out

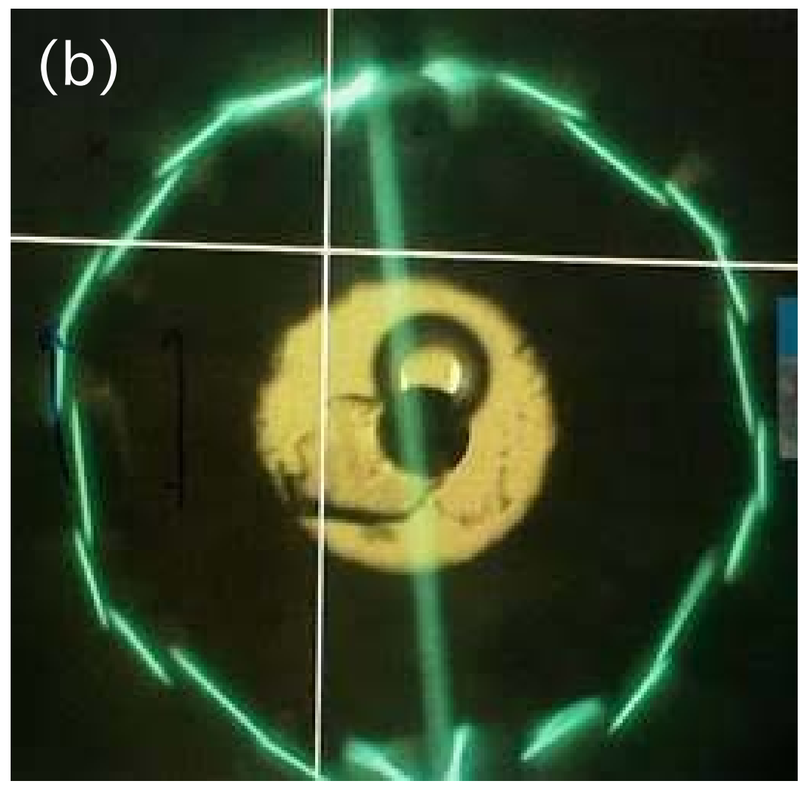
(b)

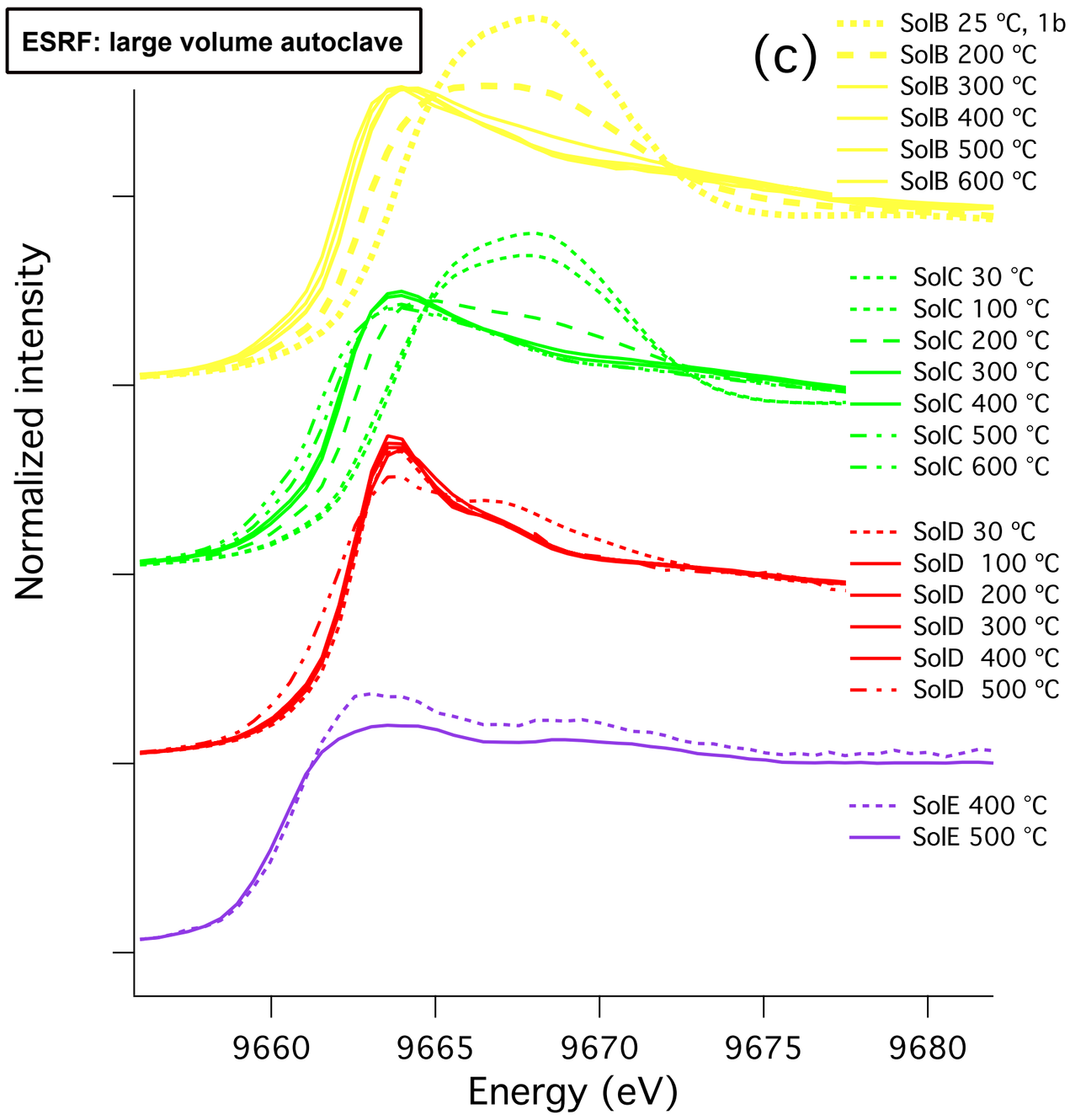
ESRF: large volume autoclave
(c)
SolB 25 °C, 1b
SolB 200 °C
SolB 300 °C
SolB 400 °C
SolB 500 °C
SolB 600 °C
SolC 30 °C
SolC 100 °C
SolC 200 °C
SolC 300 °C
SolC 400 °C
SolC 500 °C
SolC 600 °C
SolD 30 °C
SolD 100 °C
SolD 200 °C
SolD 300 °C
SolD 400 °C
SolD 500 °C
SolE 400 °C
SolE 500 °C
Normalized intensity
9660
9665
9670
9675
9680
Energy (eV)

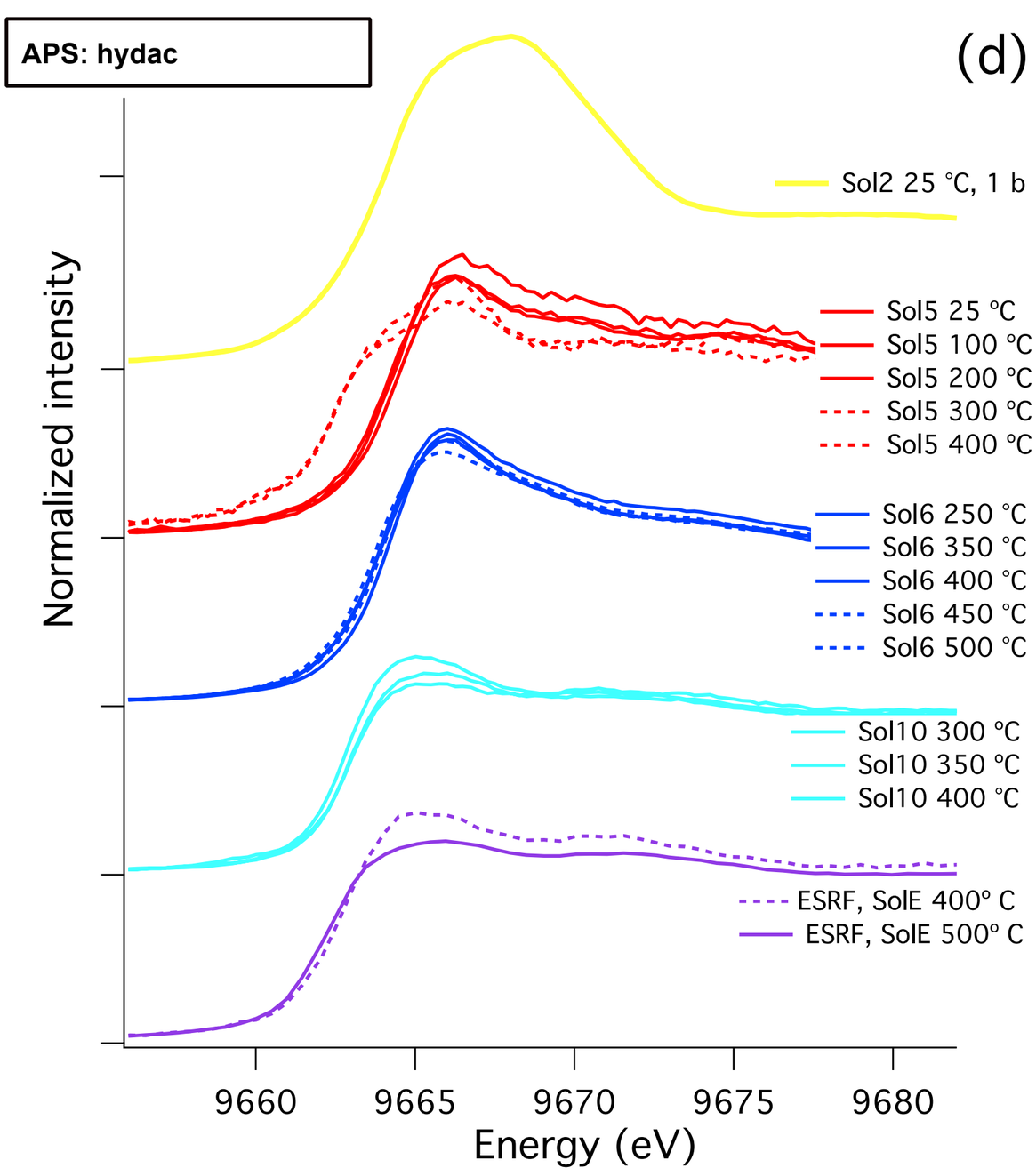
APS: hydac
(d)
Sol2 25 °C, 1 b
Sol5 25 °C
Sol5 100 °C
Sol5 200 °C
Sol5 300 °C
Sol5 400 °C
Sol6 250 °C
Sol6 350 °C
Sol6 400 °C
Sol6 450 °C
Sol6 500 °C
Sol10 300 °C
Sol10 350 °C
Sol10 400 °C
ESRF, SolE 400° C
ESRF, SolE 500° C
Normalized intensity
9660
9665
9670
9675
9680
Energy (eV)

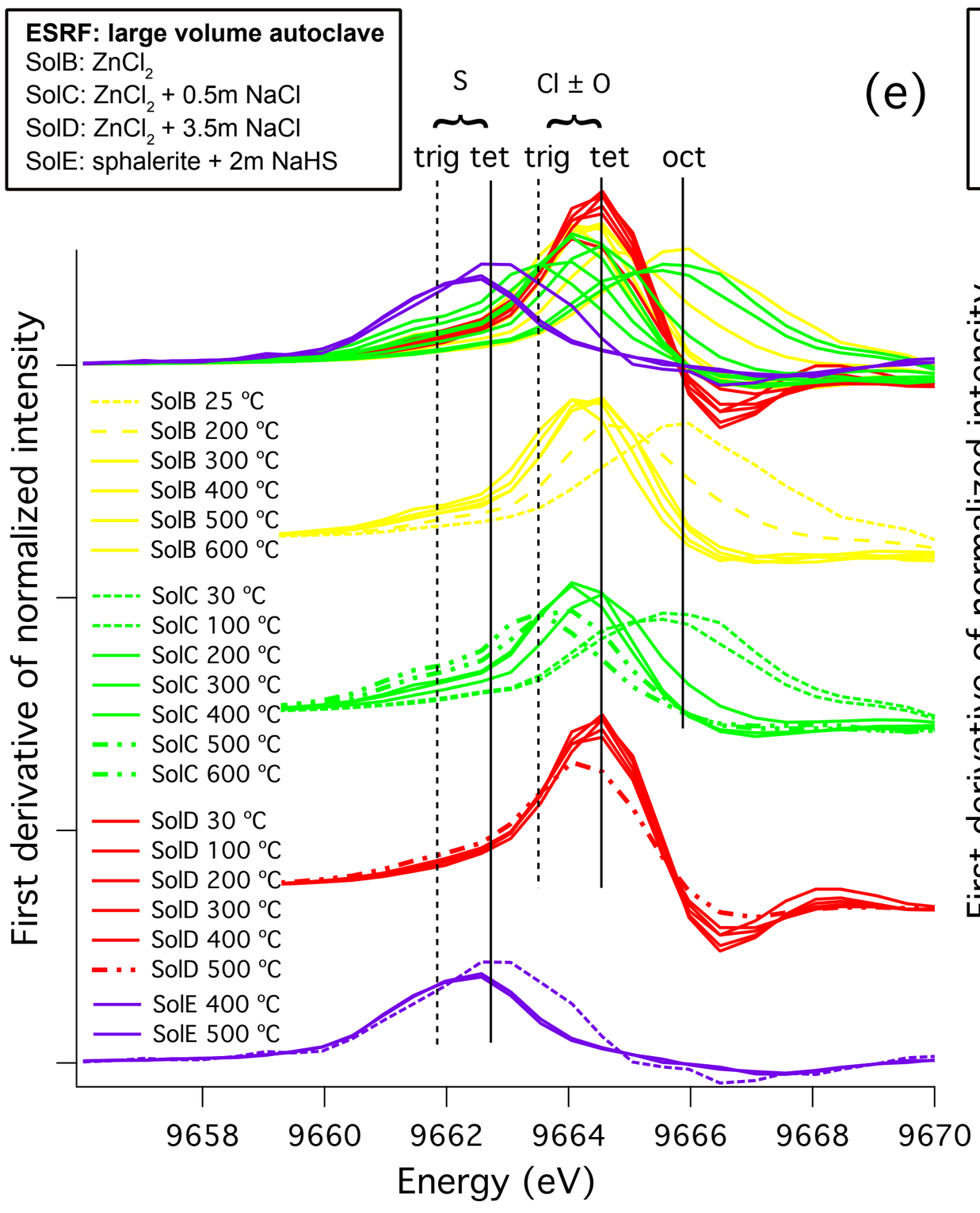
ESRF: large volume autoclave
SolB: ZnCl2
SolC: ZnCl2 + 0.5m NaCl
SolD: ZnCl2 + 3.5m NaCl
SolE: sphalerite + 2m NaHS
(e)
S
Cl ± O
trig tet trig tet oct
SolB 25 °C
SolB 200 °C
SolB 300 °C
SolB 400 °C
SolB 500 °C
SolB 600 °C
SolC 30 °C
SolC 100 °C
SolC 200 °C
SolC 300 °C
SolC 400 °C
SolC 500 °C
SolC 600 °C
SolD 30 °C
SolD 100 °C
SolD 200 °C
SolD 300 °C
SolD 400 °C
SolD 500 °C
SolE 400 °C
SolE 500 °C
First derivative of normalized intensity
9658
9660
9662
9664
9666
9668
9670
Energy (eV)

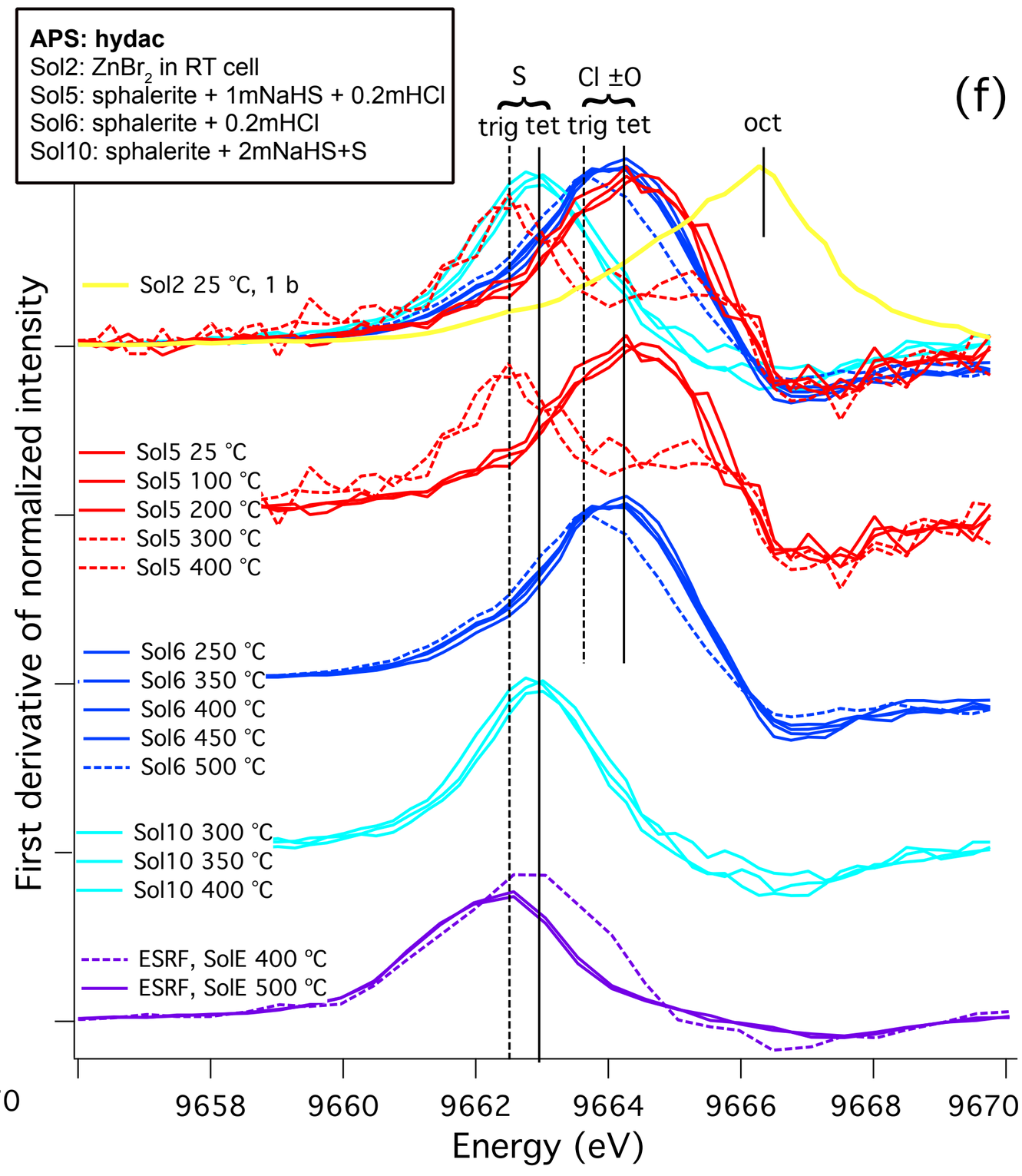
APS: hydac
Sol2: ZnBr2 in RT cell
Sol5: sphalerite + 1mNaHS + 0.2mHCl
Sol6: sphalerite + 0.2mHCl
Sol10: sphalerite + 2mNaHS+S
(f)
S
Cl ±O
trig tet trig tet oct
Sol2 25 °C, 1 b
Sol5 25 °C
Sol5 100 °C
Sol5 200 °C
Sol5 300 °C
Sol5 400 °C
Sol6 250 °C
Sol6 350 °C
Sol6 400 °C
Sol6 450 °C
Sol6 500 °C
Sol10 300 °C
Sol10 350 °C
Sol10 400 °C
ESRF, SolE 400 °C
ESRF, SolE 500 °C
First derivative of normalized intensity
9658
9660
9662
9664
9666
9668
9670
Energy (eV)